THEORETICAL AND EXPERIMENTAL ANALYSES OF 3D CONJUGATED HEAT TRANSFER PROBLEM IN AN IGBT POWER MODULE

Philippe Rollemberg d'Egmont, philippe@poli.ufrj.br
Christopher Peter Tostado, tostado@gmail.com
Kelvin Chen, kelvinchen@poli.ufrj.br
Carolina Palma Naveira Cotta, carolina@mecanica.coppe.ufrj.br
Fernando Pereira Duda, duda@mecanica.coppe.ufrj.br
Antonio Guilherme Barbosa da Cruz, aguicruz@mecanica.coppe.ufrj.br
Marcio Sampaio, marciosampaio@ufrj.br

Laboratory of Nano- and Microfluidics and Microsystems, LabMEMS, Mechanical Engineering Dept. (PEM) & Nanoengineering Dept. (PENT) – COPPE/UFRJ - Federal University of Rio de Janeiro, Rio de Janeiro, RJ, Brazil

Abstract. *Applications of high-power semi-conductor modules of IGBT (Insulated Gate Bipolar Transistor) type include railway traction, motor drives and hybrid-electric vehicles. IGBT power modules generate a considerable amount of heat from the dissipation of electric power, which is an important reliability issue to be considered since the temperature of a semiconductor device must be kept within strict limits to avoid damage. Clearly, accurate models and simulation tools are required to compute the local temperature of the devices under different load conditions of the converter. This paper describes a transient 3-D conjugated heat transfer numerical solution, which is based on the Finite Element Method, for an IGBT power device with many layers of varying cross-sectional areas, different materials and multiple heat sources. The numerical results are validated against experimental results obtained via infrared thermography, which in turn can provide a large amount of non-intrusive temperature data of the entire external surface of the IGBT modules. A good agreement regarding numerical and experimental results was observed.*

Keywords*: conjugated heat transfer, Finite Element Method, IGBT module, infrared thermography*

1. INTRODUCTION

Thermal management of electronic devices is very important since high working temperatures can be very harmful to their service life, especially for switching devices such as insulated gate bipolar transistor (IGBT), which is basically a power semiconductor device primarily used as an electronic switch that combines high-current density with fast switching (Chang *et al.*, 2016). These devices are fundamental elements of power conversion and are used extensively, for example, in variable frequency drives, electric cars and trains. The current flow in these devices induces fast temperature increase inside the module as a consequence of the Joule effect, which constitutes a serious reliability concern since the device temperature has to be controlled not to exceed a maximum pre-established value to avoid undesirable effects like the change of electrical properties, the increase of leakage current, change of the threshold voltage and commutation time (Wu *et al.*1996; Sheng *et al.*, 2000). Furthermore, it is known that high internal temperatures are responsible for multiple operational failures and also drastically reduce the reliability and the equipment life, making the thermal management extremely important for the correct operation (Luo, 2002).

In this paper, an infrared camera is used in an experiment to measure surface temperatures of an IGBT module since infrared thermography is a non-intrusive technique with high definition and low uncertainty. These temperature measurements will be compared with those obtained via numerical simulation performed in the software ANSYS. In this simulation, the temperature of the IGBT module was predicted using a 3D model in which the heating by Joule effect can be represented by boundary condition of heat flux on area of IGBT and Diode chips when the electric current passes thought them (Narumanchi et al., 2008). Multiple correlations, applicable for small Rayleigh number, were used to determine the heat transfer coefficient for each vertical, horizontal upward-facing and downward-facing plates of each component (Rohsenow, 1998; Ozisik, 1985; Kreith, 1999). A good agreement regarding numerical and experimental results was observed.

2. EXPERIMENT

Each IGBT module contains two sub-modules and each sub-module contains two chips, one diode and one IGBT chip, as detailed in the opened module (Fig. 1.a). The respective circuit diagram is shown in Fig. 1.b. As can be seen in Figure 2, the experimental setup consists in a support with an infrared camera FLIR A645Sc25° (item 1) placed on top of the IGBT module surface (item 4) to take the thermal images; two power supplies, one to stabilize the voltage between the gate and emitter (item 7), whereas the other one (item 8) provides the energy from the collector to emitter;

One oscilloscope (item 2) to measure the voltage supplied to the IGBT unit; one multimeter (item 3) as a secondary method for verifying the voltage; one current probe (item 6) to measure the current supplied and one fan (item 5) to enhance the cooling process of the IGBT unit with forced convection in between experiments.

A regulated power supply with a maximum voltage and current of 34 volts and 3 amperes was used to provide a stable voltage (gate-emitter voltage, V_{GE}) to the gate of the IGBT unit (represented as 4→5 and 6→7 in Figure 1). The other power supply was used to provide power (collector-emitter voltage, V_{CE} and current, A) from the collector to the emitter in the circuit. Due to the architectural and circuit limitations of the device, only one component could be powered at a time. Taking into account these limitations, a total of three different experimental settings were tested to determine temperature profiles in the outer surface of the IGBT unit with a constant DC voltage supplied to the gate and with approximately the same amount of power supplied to different individual components within unit.

The experimental procedure began by specifying in the camera software the key parameters such as the ambient temperature, humidity, surface emissivity, acquisition rate and distance between the camera lens and object to be measured, and setting the value of the desired voltage to be supplied by the first power supply unit to the IGBT module (represented by item 7 of Figure 1). Then the second power supply is turned on so allowing the passage of current from the first source (source represented by item 8 in Figure 1) for the IGBT drive. The surface temperatures were then measured, and once reached the steady state, the purchasing system is shut down and the sources are then turned off. The camera images are properly identified and saved for future comparisons with simulation results and/or solution of the corresponding inverse problems. Infrared images acquired by thermographic camera are treated in ResearchIR software FLIR. After each experiment, the fan (item 5 of Figure 1) was switched on to assist with the cooling of the IGBT unit and ensure that the temperature of the components to return to room temperature before beginning the next experiment.

With this setup, three experimental configurations (cases 1-3), supplying one single chip per case, were tested to determine the temperature profile on the open IGBT module surface, which was painted with graphite paint (Kontakt Chemie Graphit 33 Spray) of known emissivity of 0.97. The tree test cases are detailed in Tab. 1.

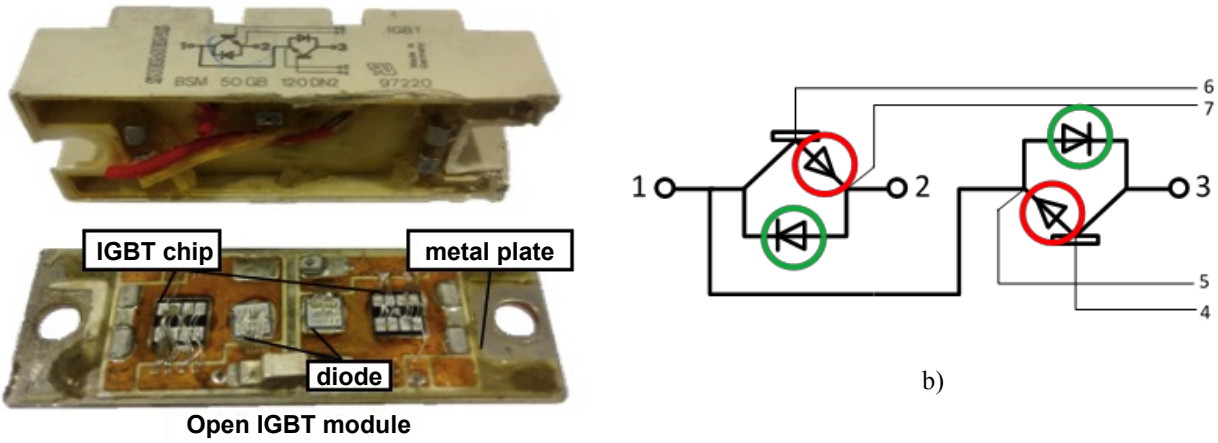

Figure 1. IGBT module (Double module Siemens BSM 50GB 120DN2): a) open and disconnected from the plastic case; b) circuit diagram, with diodes in green and IGBTs in red.

Table 1. Different experimental configurations with its input conditions.

Case	Supplied components	Current (A)	Voltage, V_{CE} (V)	Power (W)	Ambient Temperature (C)
1	Left diode	6.15 ± 0.12	1.0 ± 0.04	6.15 ± 0.12	24.9
2	Left IGBT	4.91 ± 0.10	1.25 ± 0.05	6.14 ± 0.12	24.7
3	Right diode	6.16 ± 0.12	1.0 ± 0.04	6.16 ± 0.12	24.5

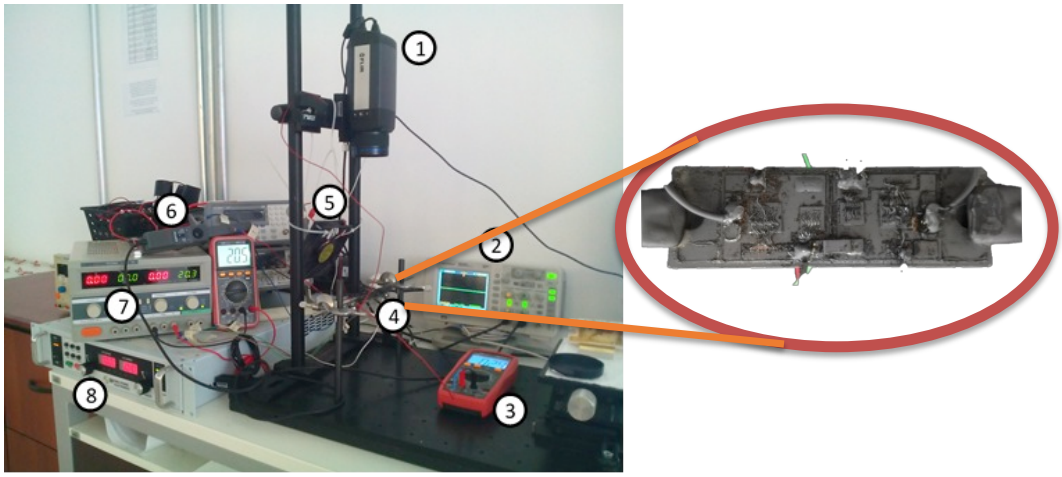

Figure 2. Experimental setup. 1- Infrared camera; 2- Oscilloscope; 3- Multimeter; 4- Siemens IGBT Module; 5- Fan; 6- Current probe; 7- Primary power supply; 8 – Secondary high current/voltage power supply.

Maximum IGBT surface temperature variation ΔT for the cases 1, 2 and 3, are presented in Fig. 3, which also illustrates some thermal images for three different times corresponding to case 2. The maximum and minimum temperatures in the infrared image are indicated by a red triangle and a blue triangle, respectively. The black rectangle delimits the area within which the temperature measurements were analyzed.

As can be seen, the temperature variation, ΔT, for the three cases are very similar, with steady state values of 44.25°C, 44.93°C, e 44.92°C, respectively. As it is illustrated through the infra red images, for a short time (5.0s), the area that corresponds to the left IGBT presents the highest temperature, as expected since this image refers to case 2, and as the time evolves (50s and 1500s), the temperature in the module tends to be more uniform since the heat is spreading to the rest of the device, but the highest temperature measured still remains in the left IGBT area. For a long time (1500s), when the steady state is almost reached, the temperature is more uniform than for lower times but the highest value still achieved in the left IGBT as expected since the heat-source is located in this chip for case 2.

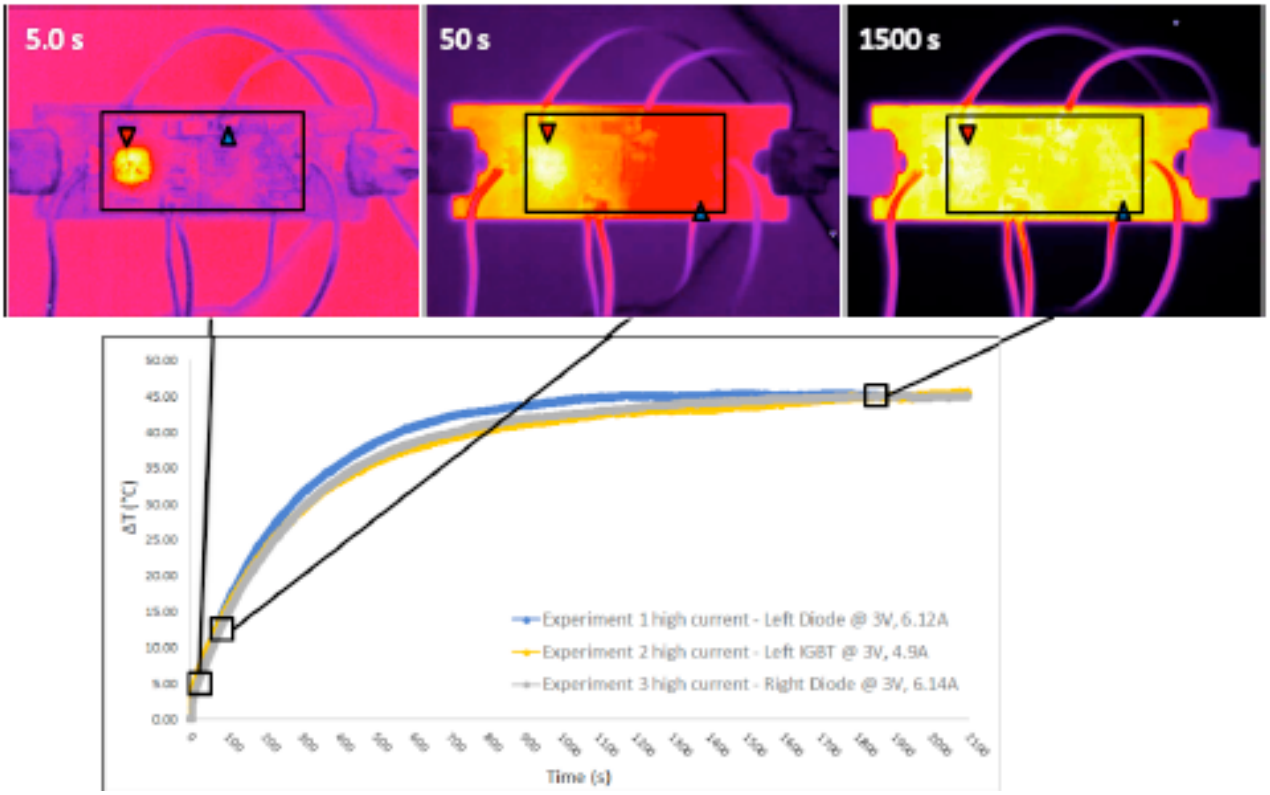

Figure 3. Maximum IGBT surface ΔT for the cases 1, 2 and 3, and illustrative infrared images from case 2 in different times (5s, 50s and 1500s).

3. THERMAL MODEL

3.1 Computational domain

The computational domain used in the mathematical formulation is described by the Fig. 4 that shows details of the 3D geometry, highlighting by different colors the materials of each component that compose the IGBT module. The properties of each material are described in Tab. 2, with the values taken from the literature (Liao *et al.*, 2014; Occhionero *et al.*, 2002). The thickness of each material layer and the dimensions were obtained using a caliper rule and a digital microscopy. The geometry was created using CAD software.

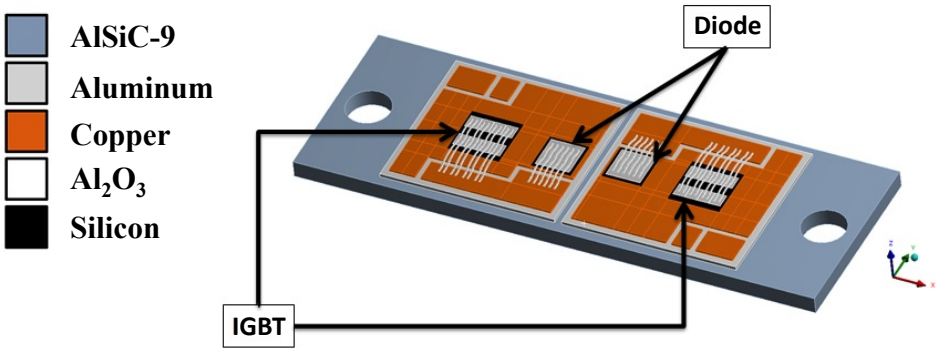

Figure 4. Material that compose the IGBT module.

Table 2. Properties of the different materials.

Material	Thickness (mm)	Density (kg/m³)	Specific heat (J/kgK)	Thermal Conductivity (W/mK)
Aluminum	0.036	2700	900	237
Silicon (IGBT)	0.309	2330	700	148
Silicon (Diode)	0.314	2330	700	148
Copper	0.286	8920	380	400
Al_2O_3	0.668	2320	1040	1.7
AlSiC-9	3.000	3000	434	393

The energy equation and the initial condition for the temperature in the whole IGBT module domain Ω presented in Figure 4 can be written as:

$$\rho c \frac{\partial T(\mathbf{x},t)}{\partial t} = \nabla \cdot \mathbf{q} + Q(\mathbf{x},t), \quad \mathbf{q} = -k\nabla T \ \text{ in } \ \Omega \tag{1}$$

$$T(\mathbf{x},0) = T_0(\mathbf{x}) \ \text{ in } \ \Omega \tag{2}$$

where ρ is the density, c is the specific heat, k is the thermal conductivity, $\mathbf{q}$ is the heat flux, T is the temperature, t is the time, $\mathbf{x}$ is the position vector, Q is the heat-source generated by the Joule effect and T_0 is the initial temperature.

3.2 Boundary conditions

The proper boundary conditions that could be representative of the experimental results of case 2, from Table1, described previously are here detailed. It was adopted a total power of 6.14 W applied on the region highlighted in blue in Fig. 5, where the left IGBT chip is situated and which has a surface area of 79.21 mm². The heat losses of the entire boundaries were considered to occur by natural convection and radiation.

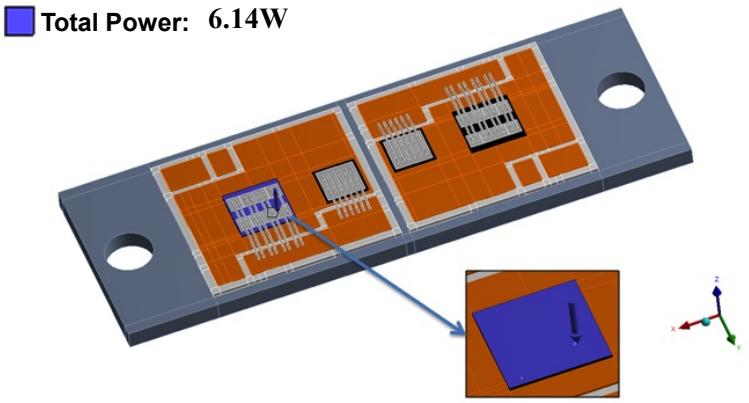

Figure 5. Total power applied on the left IGBT area.

The radiation was modeled using the emissivity value of 0.97 on the top surface of the IGBT module (Fig. 6.b), since this top face was painted with the graphite paint with the known emissivity. For the remaining surfaces, which are not painted, were adopted an emissivity value of 0.05 at room temperature (Fig. 6.a), referring to a polished metal (Minkina and Dudzik, 2009).

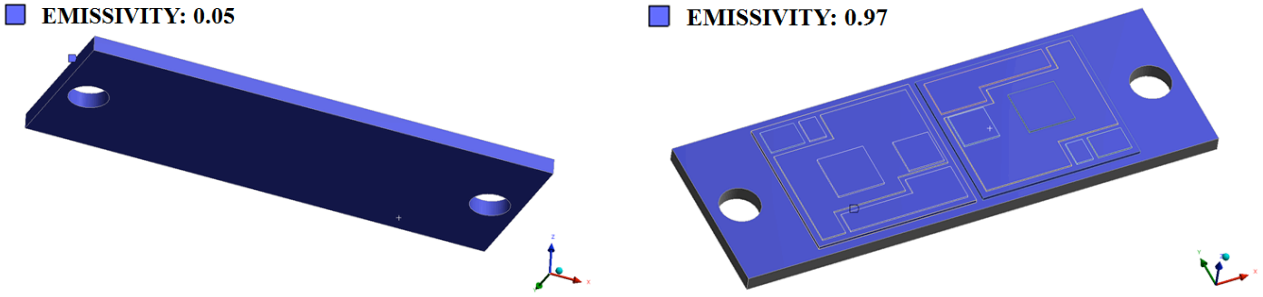

a) b)

Figure 6. Surfaces with different emissivity.

To model the heat transfer by natural convection with the environment, it was necessary to use empiric correlations to estimate the heat transfer coefficient. The correlations adopted (Ozisik, 1985; Rohsenow, Hartnett and Cho, 1998; Kreith, 1999) are valid for a large range of Rayleigh numbers. The convective heat transfer (h_1 until h_8) varying with surface temperature was calculated from the following correlations for horizontal heated upward-facing plates at a constant room temperature of 25 ºC. The following equation (3) applies for $1 < \mathrm{Ra} < 10^{10}$ (Rohsenow, 1998), where h is the convective heat transfer coefficient, k_{air} is the thermal conductivity of the air, Ra is the Rayleigh number, T_s is the heated surface temperature, T_r is the room temperature, v is the kinematic viscosity of air, g is the acceleration due to gravity, Pr is the Prandtl number, α is the thermal diffusivity of air, L is the characteristic length, defined by the ratio between the area and perimeter of each geometry (as detailed in Tab. 3), m is equal to 10 as chosen by Rohsenow et al. in order to provide the best fit to the their experimental data for horizontal heated upward-facing plates. $\mathrm{Nu_t}$ is the turbulent Nusselt number, Nu_ℓ is the laminar Nusselt number, $\mathrm{Nu^T}$ is the laminar thin layer. $\mathrm{C_t^U}$ and C_ℓ are parameters that depends on the Prandtl number.

$$h = \mathrm{Nu}\frac{k_{\mathrm{air}}}{L} \qquad \mathrm{Nu} = \left((\mathrm{Nu}_\ell)^m + (\mathrm{Nu_t})^m\right)^{1/m};$$

where : (3.a-g)

$$\mathrm{Nu}_\ell = \frac{1{,}4}{\ln(1+1{,}4/\mathrm{Nu^T})}; \qquad \mathrm{Nu^T} = 0{,}0835\,\mathrm{C}_\ell\,\mathrm{Ra}^{1/2}; \qquad \mathrm{C}_\ell = \frac{0{,}0671}{\left(1+(0{,}492/\mathrm{Pr})^{9/16}\right)^{4/9}}$$

$$\mathrm{Nu_t} = \mathrm{C_t^U Ra}^{1/3}; \qquad \mathrm{Ra} = \frac{2gL^3}{\nu^2}\frac{(\mathrm{T_s}-\mathrm{T_r})}{(\mathrm{T_s}+\mathrm{T_r})} \qquad \mathrm{C_t^U} = 0{,}14\left(\frac{1+0{,}0107}{1+0{,}01\mathrm{Pr}}\right); \qquad \mathrm{Pr} = \frac{\nu}{\alpha}$$

The horizontal surfaces facing up were separated in eight regions. The eight different sub-surfaces are described in Fig. 7 and the details of each sub-surface are described in Tab. 3. Fig. 8 depicts the convective heat transfer coefficient variation in the range of temperature from 25C to 80C, for each sub-surface, according to the presented Rohsenow, Hartnett and Cho (1998) correlation.

Table 4. Details of each sub-surface facing up and surface facing down.

Sub-surface	Base	Al_2O_3	Copper 1	Copper 2	Copper 3	Copper 4	Diode	IGBT	Base (bottom)
Conv. Heat Transf. Coefficient	h_1	h_2	h_3	h_4	h_5	h_6	h_7	h_8	h_{14}
Area [m^2]	0,00107	1,8159E-04	1,5040E-05	3,0550E-05	1,1936E-04	3,8481E-04	4,62E-05	7,9210E-05	2,7834E-03
Perimeter [m]	0,52795	0,3234	1,5800E-02	0,0224	6,0000E-02	0,1708	2,72E-02	3,560E-02	0,29355
L [m]	0,002026	0,0005615	0,0009519	0,00136384	0,0019893	0,002253	0,0017	0,002225	0,00948186

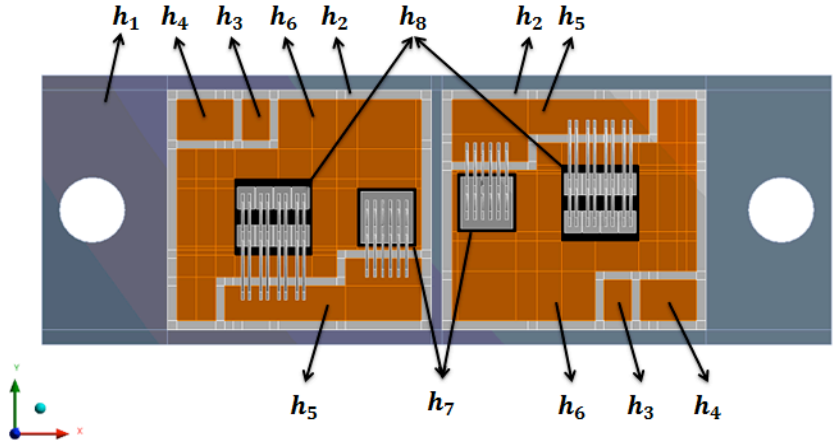

Figure 7. Top view of the IGBT module showing the different heat transfer coefficient, *h,* for each surface facing up.

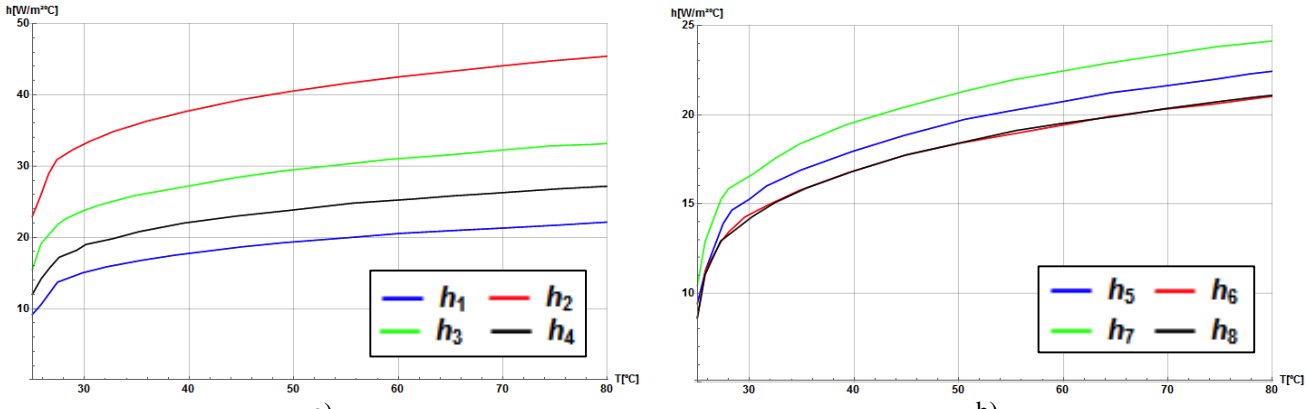

a) b)

Figure 8. Convective heat transfer coefficient varying with temperature for the different sub-surfaces facing up on the IGBT module: a) h_1, h_2, h_3 and h_4; b) h_5, h_6, h_7 and h_8.

Equation (4) shows the correlations of the convective heat transfer coefficient (h_9 until h_{13}) for vertical plates at a constant room temperature of 25 ºC and a variable surface temperature, adopted for all vertical surfaces of the IGBT module. The following equation applies for $10^{-1} < \mathrm{Ra} < 10^{9}$ (Ozisik, 1985).

$$h = \mathrm{Nu}_m \frac{k_{air}}{L}; \qquad \mathrm{Nu}_m^{1/2} = 0{,}825 + \frac{0{,}387\mathrm{Ra}^{1/6}}{\left(1+(0{,}492/\mathrm{Pr})^{9/16}\right)^{8/27}}; \tag{4.a-b}$$

where Nu_m is value of mean Nusselt number.

As Fig. 9 indicates, the convective heat transfer coefficients corresponding to the five types of vertical sub-surfaces here considered are named from h_9 to h_{13}. For the only surface facing down on the IGBT module (bottom surface of the base of AlSiC-9), the convective heat transfer is named as h_{14}. The details of each vertical and bottom sub-surface are provided in Tab. 3 and Tab. 4. The convective heat transfer coefficient (h_{14}) varying with surface temperature was calculated from the following correlations for horizontal heated downward-facing plates at a constant room temperature of 25 ºC. The following equation (5) applies for $\mathrm{Ra} < 10^{10}$ (Kreith, 1999), where H_ℓ is a parameter that depends on the Prandtl number:

$$h = \mathrm{Nu}\frac{k_{\mathrm{air}}}{L} \qquad \mathrm{Nu} = \frac{2{,}45}{\ln\left(1+2{,}45/\mathrm{Nu}^{\mathrm{T}}\right)};$$
$$\mathrm{Nu}^{\mathrm{T}} = \mathrm{H}_\ell \mathrm{Ra}^{1/5}; \qquad \mathrm{H}_\ell = \frac{0{,}527}{\left(1+(1{,}9/\mathrm{Pr})^{9/10}\right)^{2/9}}; \tag{5.a-d}$$

The results for the convective heat transfer coefficient for each vertical and bottom sub-surface, varying with the temperature, obtained with the respective correlation of vertical sub-surface and bottom face are shown in Fig. 10.

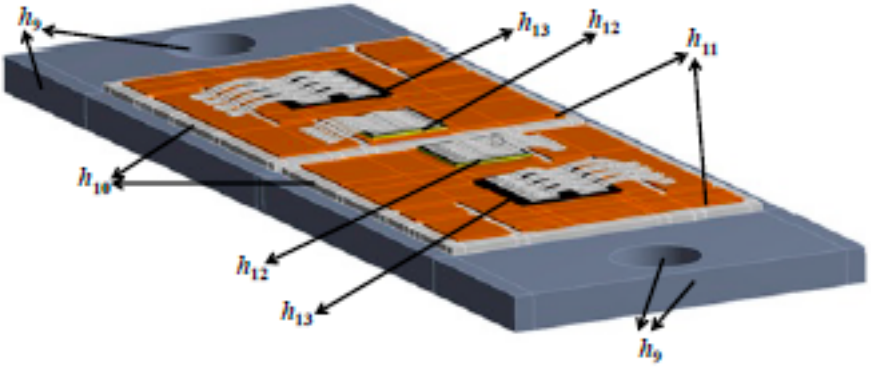

Figure 9. Different *h* for each vertical surface of the IGBT module.

Table 4. Details of the heat transfer coefficient, *h,* for each vertical surface.

Sub-surface	Base (vertical)	Al_2O_3	Copper	Diode	IGBT
Conv. Heat Transf. Coefficient	h_9	h_{10}	h_{11}	h_{12}	h_{13}
L [mm]	3.000	0.668	0.286	0.314	0.309

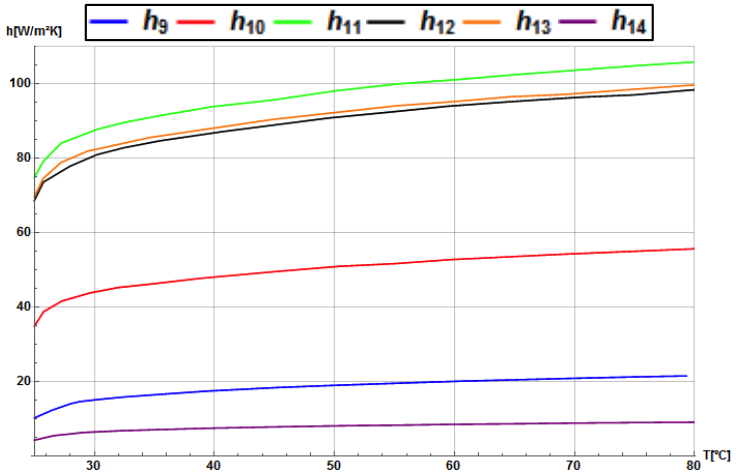

Figure 10. Convective heat transfer coefficient varying with temperature for the different vertical sub-surfaces and horizontal bottom surface (facing down) of the IGBT module.

For the initial condition for the whole IGBT module domain was adopted the ambient temperature of 25 ºC since it was assumed the module was in thermal equilibrium with the environment at the beginning of the experiments.

4. NUMERICAL SIMULATION

The mathematical model developed previously was discretized by the finite element method using the software ANSYS. First, it is necessary a study of mesh convergence in order to ensure that the mesh size will not interfere in the results. For the mesh convergence analysis, five different meshes were built. The mesh 1 is the coarser one, whereas the mesh 5 is the finer one, *i.e.*, with the most elements quantity. Figures 11 and 12 show a study of mesh sensibility regarding the maximum global temperature, minimum global temperature and maximum temperature in the IGBT module base. Based on the graphics analyses of the mesh sensitivity shown in Fig. 11 and 12, the mesh 5 with temporal discretization of 131 number of points was chosen to the final simulations due to the lower relative error presented. Figure 13 displays the mesh 5 chosen to be used in further simulations. Mesh 5, contains 100380 nodes and 14452 elements. It has a better refinement in the region of the IGBT chip, where heat generation takes place by the Joule effect and where by higher temperature gradients are expected.

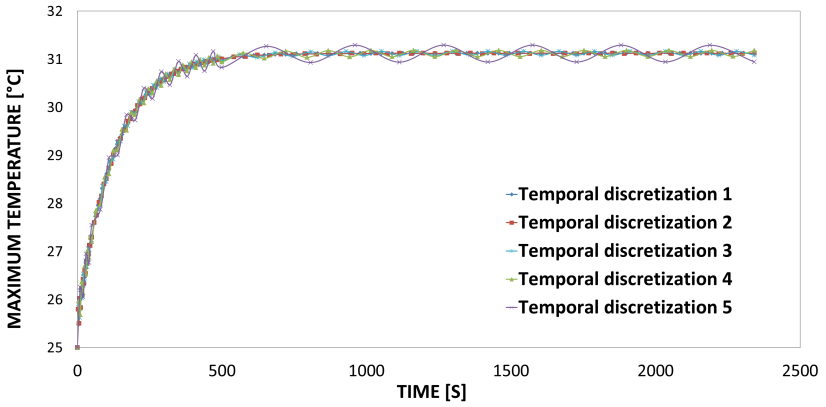

Figure 11. Global maximum temperature over the time for different temporal discretization.

Table 5. Sensibility of the temporal discretization.

Temporal disc.	Number of points	Rel. error for the max. temp. (%)
1	131	0.000289
2	118	0.000514
3	79	0.000900
4	66	0.003111

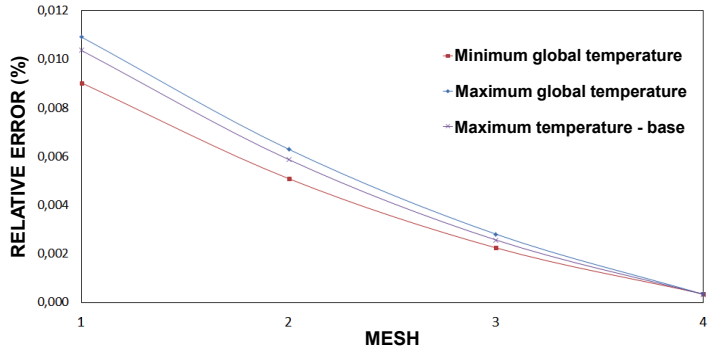

Figure 12. Mesh sensitivity. Relative error of the temperatures for different meshes.

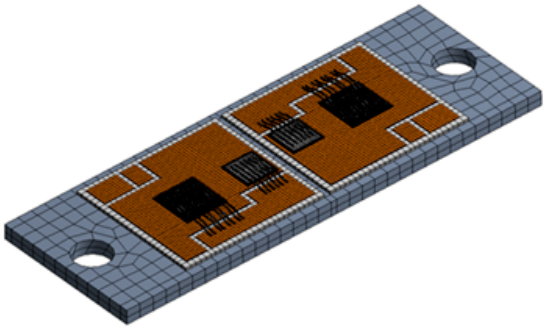

Figure13. Mesh 5 used in the final simulations.

5. RESULTS

Numerical simulations of the thermal model described previously were performed after defining all the convective heat transfer coefficients for all the surfaces of the IGBT module as detailed in the previous section. With the radiation properties and the initial condition also presented previously, all the necessary conditions to run the simulation are defined. The simulation performed used the properties described in Tab. 2 and the boundary conditions mentioned before in order to represent the experiment of case 2 from the Tab. 1. Fig. 14 shows the results for temperature distribution over the IGBT module at 2342 seconds. As we can see, the maximum temperature of 70,278 °C, is located mainly on the left wires, pads and IGBT while the minimum temperature 61,168 °C is located mainly on the right side of module. Figure 15 shows the comparison of the numerical and experimental results for the maximum temperature varying with time for the case 2 described in Tab. 1.

The comparison presented in Fig. 15 shows that before reaching the steady state, a higher discrepancy between numerical and experimental results is characterized by a relative error of about 16% at 158 seconds. This difference may be due to non-characterization of electrical effects in the presented model. Nevertheless, a relatively good agreement was observed when steady-state was reached, since the maximum global temperature for the experimental results was 70,686 °C, while the maximum global temperature for the numerical results was 70,278 °C, representing a relative error of about 0,58 %.

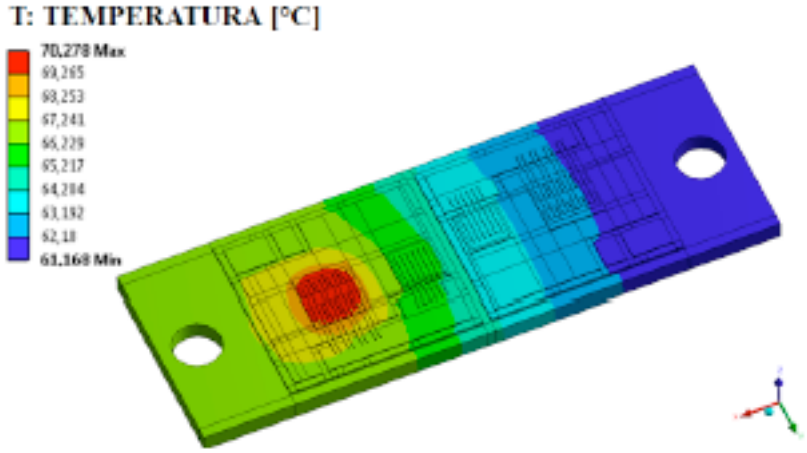

Figure 11. Temperature distribution at time 2342 s obtained via numerical simulation.

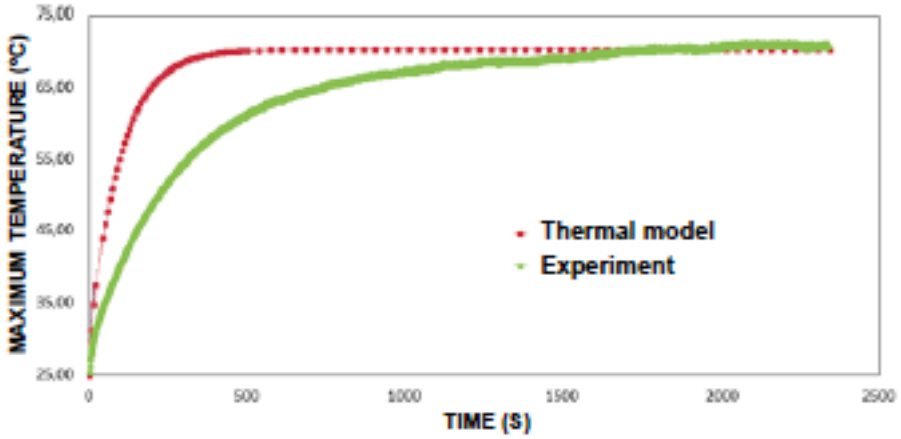

Figure 12. Comparison between the numerical and experimental results for the maximum.

6. ACKNOWLEDGEMENTS

The authors acknowledge the financial support of the sponsoring agencies FAPERJ and GE- General Electric Company.

7. REFERENCES

Batard, C., Ginot N., and Antonios J., "Lumped dynamic electrothermal model of IGBT module of inverters", IEEE Trans. Compon. Packag. Manuf. Technol., vol. 5, no. 3, pp. 355-364, 2015.

Chang, T. C., Fuh, Y. K., Lu, H. Y., Tu, S. X., 2016. "Thermal management and performance evaluation of a dual bi-directional, soft-switched igbt-based inverter for the 1st autonomous microgrid power system in taiwan under various operating conditions". Heat and Mass Transfer, Vol. 52, No. 6, pp. 1231–1241.

Kreith, F., 1999. Heat and Mass Transfer - Mechanical Engineering Handbook. CRC Press, Boca Raton.

Liao, L. L., Hung, T. Y., Liu, C. K., Li, W., Dai, M. J., Chiang, K. N., 2014. "Electro-thermal finite element analysis and verification of power module with aluminum wire". Microelectronic Engineering, Vol. 120, pp. 114-120.

Luo, Z., 2002. A thermal model for igbt modules and its implementation in a real time simulator. Ph.D. thesis, University of Pittsburgh, Pittsburgh, PA, USA.

Minkina, W., S. Dudzik, S., 2009. Infrared Thermography: Errors and Uncertainties. Wiley, New York.

Narumanchi, S., Mihalic, M., Kelly, K., and Eesley, G., "Thermal interface materials for power electronics applications, " ITHERM 2008, May 28- 31, 2008.

Occhionero, M. A., Fennessy, K. P., Adams, R. W., Sundberg, G. J., 2002. "Alsic baseplates for power IGBT modules: design, performance and reliability". In Proceedings of Process Conversion Intelligent Motion 172.

Ozisik, M.N., 1985. Heat Transfer – A Basic Approach. McGraw Hill, New York.

Rohsenow, W. M., Hartnett, J. P., Cho, Y. I., 1998. Handbook of heat transfer. McGraw-Hill, New York.

Wu, W.; Gao, G.; Dong, L.; Wang, Z.; Held, M.; Jacob, P.; Scacco, P., 1996. "Thermal reliability of power insulated gate bipolar transistor (IGBT) modules". In proceedings of the Semiconductor Thermal Measurement and Management Symposium, pp. 136–141

8. RESPONSIBILITY NOTICE

The authors are the only responsible for the printed material included in this paper.